

Finite temperature correlations in the Bose-Hubbard model: application of the Gauge P representation

Saeed Ghanbari,¹ Joel F. Corney,² and Tien D. Kieu¹

¹*Centre for Atom Optics and Ultrafast Spectroscopy and ARC Centre of Excellence for Quantum-Atom Optics, Swinburne University of Technology, Melbourne, Australia**

²*ARC Centre of Excellence for Quantum Atom Optics, The University of Queensland, Brisbane, QLD 4072, Australia*
(Dated: October 28, 2021)

We study ultracold Bose gases in periodic potentials as described by the Bose-Hubbard model. In 1D and at finite temperature, we simulate ultracold Bose gases in imaginary time with the gauge P representation. We study various quantities including the Luttinger parameter K , which is important for locating the boundaries of the Mott insulator lobes, and find a simple relation for the kinetic energy part of the Bose-Hubbard Hamiltonian. We show that for $J = 0$, the stepwise pattern of the average number of particles per lattice site versus the chemical potential vanishes at temperatures above $T \approx 0.1U$. Also, at chemical potential $\mu = 0.5U$ and temperature $T = 0.5U$ by increasing J , the relative value of the number fluctuation decreases and approaches that of a coherent state.

PACS numbers: 03.75.Lm,37.10.Gh,37.10.Jk,67.85.-d,73.43.Nq,42.50.Lc,05.10.Gg,05.30.Jp
Keywords:

We investigate quantum degenerate Bose gases at finite temperature in the grand canonical ensemble [1] and use the Bose-Hubbard model which can describe the dynamics of ultracold atoms in periodic potentials such as optical [2, 3, 4] and magnetic lattices [5, 6, 7, 8, 9, 10]. A superfluid of ultracold bosons trapped in a periodic lattice undergoes a superfluid to Mott insulator quantum phase transition if the barrier height between the lattice sites is adiabatically increased [2, 3, 4]. In the Mott insulator phase there is a fixed number of atoms per lattice site which may have applications in quantum computation [2, 3]. The Bose-Hubbard model is also important for the study of systems with strongly correlated bosons [11].

Ultracold bosons at zero temperature in the Bose-Hubbard model have been studied using different methods such as Monte Carlo simulations [12, 13, 14, 15], mean field theory [16, 17, 18], Bethe-Ansatz solution [19], exact diagonalization [20], strong-coupling expansions [21], density-matrix renormalization group (DMRG) (infinite-size) [22], DMRG (finite-size) [23] and exact diagonalization plus renormalization group [24]. DMRG [23] gives high precision results in only one dimensional many-body problems [25, 26]. Bose-Hubbard model at finite temperature has been considered via mean-field theory [16, 27, 28], Monte Carlo simulations of a quantum rotor model [29], an *ab initio* stochastic method [30], perturbative DMRG [31] and slave particle techniques [32]. So far, most of the finite temperature studies on the Bose-Hubbard model have been based on perturbation theory or some approximations.

In this paper we use gauge P representation which is an exact phase space method based on a coherent state

representation. We promote the use of gauge P representation as an exact method to benchmark various approximate methods and simplifying assumptions. We evaluate the performance of this method for these imaginary time calculations of the Bose-Hubbard model to calculate correlations at finite temperature to connect between the different limiting cases. Applying a phase space method for a system with a Hamiltonian written in the second quantized form, it is possible to convert the master equation of the system (such as the Liouville-von Neumann equation) into a differential equation [33]. Phase space methods such as positive P representation [34] and gauge P representation [35] can give accurate results which their accuracy depends on the number of simulation trajectories. Using the gauge P representation, the second-order spatial correlation function and also momentum distribution have been calculated for an interacting 1D degenerate Bose gas in the Bose-Hubbard model [1]. We investigate ultracold atoms at finite temperatures with the gauge P representation [35] and open boundary conditions. We choose the gauge P representation over other quantum phase space methods including the positive P representation [34] because in studying the many-body physics problems with strongly correlated bosons, the gauge P representation gives more stable results and also the sampling error is reduced, compared with the positive P representation [36, 37]. Furthermore, the positive P /gauge P is exact, whereas other phase-space methods are not.

We have verified the gauge P technique by comparisons with exact numerical and also analytical results in simple cases [38]. Our simulation results are, within the sampling error, in remarkable agreement with the known limiting cases when either the hopping matrix element J or the onsite interaction U is zero. Therefore, they could be considered as a touchstone for testing the reliability of approximate techniques when both J and U

*Electronic address: sghanbari@swin.edu.au

are nonzero. Nevertheless, with the present gauge in the gauge P representation, because of increase in sampling error, simulation results for the the physical quantities in the Bose-Hubbard model are not precise at temperatures below $T = 0.05U$, when both J and U have finite values.

In 1D, we simulate ultracold atoms in the Bose-Hubbard model with up to 11 lattice sites and study the average number of particles and coherence between lattice sites at finite temperatures. We show that for 11 lattice sites, the edge effects are not very important and for a Bose-Hubbard model with 11 sites, we calculate the Luttinger liquid parameter which is important for locating the boundaries of the Mott insulator lobes [39, 40, 41].

The Bose-Hubbard Hamiltonian is [2, 3]

$$\hat{H} = -J \sum_{\langle i,j \rangle} \hat{a}_i^\dagger \hat{a}_j + \frac{1}{2}U \sum_{i=1}^M \hat{n}_i(\hat{n}_i - 1) + \sum_{i=1}^M \epsilon_i \hat{n}_i, \quad (1)$$

where M is the number of lattice sites and $\langle i, j \rangle$ means that the summation is taken over adjacent sites only. Also, \hat{a}_i^\dagger , \hat{a}_i and $\hat{n}_i = \hat{a}_i^\dagger \hat{a}_i$ are creation, annihilation and number operators, respectively. The canonical commutation relations for \hat{a}_i and \hat{a}_j^\dagger are $[\hat{a}_i, \hat{a}_j^\dagger] = \delta_{ij}$. The hopping matrix element J is defined by $J = -\int d^3\mathbf{x} w^*(\mathbf{x} - \mathbf{x}_i) [-\hbar^2/2m\nabla^2 + V_0(\mathbf{x})] w(\mathbf{x} - \mathbf{x}_j)$, where V_0 is a periodic potential like the optical lattice (see [42], for a review on optical lattices) or the magnetic lattice [5, 6, 10] potential. Wannier functions $w(\mathbf{x} - \mathbf{x}_i)$ are localized position eigenstates [43]. The on-site interaction $U = g \int d^3\mathbf{x} |w(\mathbf{x})|^4$, where $g = 4\pi a_s \hbar^2/m$ and a_s and m are the s-wave scattering length and mass of the bosonic atom, respectively.

At zero temperature, if $U \gg J$, the system is well into the Mott insulator (MI) regime. For the Mott insulator with the commensurate filling of $n_i = n = N/M$, where n_i are the number of particles per lattice site, the ground state of the system for $J = 0$ is described by $|\Psi_{MI}\rangle_{J=0} = |n, \dots, n\rangle$ [44]. Atom-atom correlations $C_i(r)$ [22, 23, 45] and density-density correlations $D_i(r)$ [45] are defined by $C_i(r) = \langle \hat{a}_i^\dagger \hat{a}_{i+r} \rangle$ and $D_i(r) = \langle \hat{n}_i \hat{n}_{i+r} \rangle$, where r is an integer and $0 < r < M$. The standard deviation of the number of particles [63] is $\Delta n_i = \sqrt{\langle \hat{n}_i^2 \rangle - \langle \hat{n}_i \rangle^2}$. For the ground state given by $|\Psi_{MI}\rangle_{J=0} = |n, \dots, n\rangle$, the atom-atom correlations, the density-density correlations and the standard deviations at each site are $C_i(r) = 0$, $D_i(r) = n^2$ and $\Delta n_i = 0$ [45], respectively. For a Mott insulator with $J \neq 0$, according to first-order perturbation theory, we have $\Delta n_i = J/U \sqrt{4dn(n+1)}$ [46], where d and n are the dimension of the system and the average number of particles in a Mott insulator lobe, respectively.

At zero temperature, when the on-site interaction U is very small compared with the hopping matrix element J , the system is a superfluid (SF) and the ground state for $U = 0$ can be given as a coherent state $|\Psi_{SF}\rangle_{U=0} = \sqrt{N!/M^N} \sum_{\{n_i\}} |n_1, \dots, n_M\rangle / \sqrt{n_1! \dots n_M!}$ [45], where $\sum_i n_i = N$ is the total number of particles. Also, the

sum extends over all sets of occupation numbers $\{n_i\}$ subject to $0 \leq n_i \leq N$. For $M \gg 1$ and commensurate filling $N/M = 1$, we obtain $C_i(r) = 1$, $D_i(r) = 1$ and $\Delta n_i = 1$ [45]. Therefore, for the commensurate filling of $n = 1$ we have the same density-density correlations $D_i(r) = 1$ for both the superfluid and the Mott insulator ground states.

I. FORMALISM OF THE GAUGE P REPRESENTATION AND DERIVATION OF ÎTO STOCHASTIC EQUATIONS

In this section, we perform some calculations in the positive P representation and finally write the Îto form of the Langevin equations in the gauge P representation. Then, in section II we give the simulation results. Also, in this section to obtain some general expressions valid for both cases where $U \neq 0$ and $U = 0$, using the Boltzmann constant $k_B = 1$, we define dimensionless imaginary times $\tau = U/T$ for $U \neq 0$ and $\tau' = J/T$ for $U = 0$ and $J \neq 0$

Now, we consider the unnormalized density matrix $\hat{\rho}_u = e^{-(\hat{H}\tau - \mu\hat{N}\tau)}$, which is in the grand canonical ensemble, and take its derivative with respect to $\tau = U/T$ [1]

$$\frac{\partial \hat{\rho}_u}{\partial \tau} = -\frac{1}{2} \left[\hat{H} - \mu_e \hat{N}, \hat{\rho}_u \right]_+ \quad (2)$$

where $[\hat{A}, \hat{B}]_+ = \hat{A}\hat{B} + \hat{B}\hat{A}$ is the anticommutator of \hat{A} and \hat{B} . Also, μ_e is defined by

$$\mu_e = \frac{\partial[\tau\mu(\tau)]}{\partial \tau} \quad (3)$$

We now have

$$\frac{\partial \hat{\rho}_u}{\partial \tau} = -\frac{1}{2} \left[\hat{H}'(\hat{\mathbf{a}}, \hat{\mathbf{a}}^\dagger) \hat{\rho}_u + \hat{\rho}_u \hat{H}'(\hat{\mathbf{a}}, \hat{\mathbf{a}}^\dagger) \right] \quad (4)$$

where

$$\hat{H}'(\hat{\mathbf{a}}, \hat{\mathbf{a}}^\dagger) = \hat{H}(\hat{\mathbf{a}}, \hat{\mathbf{a}}^\dagger) - \mu_e \sum_{i=1}^M \hat{a}_i^\dagger \hat{a}_i \quad (5)$$

According to Eq. (B1), in the positive P representation, we have

$$\hat{\rho}_u = \int P(\boldsymbol{\alpha}, \boldsymbol{\beta}, \tau) \hat{\Lambda} d^{4M} \vec{\lambda} \quad (6)$$

Taking the derivative of Eq. (6) with respect to τ and considering Eq. (4) and Eq. (6), we obtain

$$\begin{aligned} \int \frac{\partial P(\boldsymbol{\alpha}, \boldsymbol{\beta}, \tau)}{\partial \tau} \hat{\Lambda} d^{4M} \vec{\lambda} = & \\ -\frac{1}{2} \int P(\boldsymbol{\alpha}, \boldsymbol{\beta}, \tau) \hat{H}'(\hat{\mathbf{a}}, \hat{\mathbf{a}}^\dagger) \hat{\Lambda} d^{4M} \vec{\lambda} & \\ + \frac{1}{2} \int P(\boldsymbol{\alpha}, \boldsymbol{\beta}, \tau) \hat{\Lambda} \hat{H}'(\hat{\mathbf{a}}, \hat{\mathbf{a}}^\dagger) d^{4M} \vec{\lambda} & \end{aligned} \quad (7)$$

We have, from Eq. (A4), $\hat{H}'_N(\hat{\mathbf{a}}, \hat{\mathbf{a}}^\dagger)\hat{\Lambda} = \hat{H}'_A(\boldsymbol{\alpha}, \boldsymbol{\beta} + \partial\boldsymbol{\alpha})\hat{\Lambda}$ and $\hat{\Lambda}\hat{H}'_N(\hat{\mathbf{a}}, \hat{\mathbf{a}}^\dagger) = \hat{H}'_N(\boldsymbol{\alpha} + \partial\boldsymbol{\beta}, \boldsymbol{\beta})\hat{\Lambda}$ where

$$\hat{H}'_N(\hat{\mathbf{a}}, \hat{\mathbf{a}}^\dagger) = -J \sum_{\langle i,j \rangle} \hat{a}_i^\dagger \hat{a}_j + \frac{1}{2}U \sum_{i=1}^M \hat{a}_i^{\dagger 2} \hat{a}_i^2 - \mu_e \sum_{i=1}^M \hat{a}_i^\dagger \hat{a}_i \quad (8)$$

$$\hat{H}'_A(\hat{\mathbf{a}}, \hat{\mathbf{a}}^\dagger) = -J \sum_{\langle i,j \rangle} \hat{a}_i \hat{a}_j^\dagger + \frac{1}{2}U \sum_{i=1}^M \hat{a}_i^2 \hat{a}_i^{\dagger 2} - \mu_e \sum_{i=1}^M \hat{a}_i \hat{a}_i^\dagger. \quad (9)$$

So

$$\int \frac{\partial P(\boldsymbol{\alpha}, \boldsymbol{\beta}, \tau)}{\partial \tau} \hat{\Lambda} d^{4M} \vec{\lambda} = \int P(\boldsymbol{\alpha}, \boldsymbol{\beta}, \tau) \mathcal{L}_A^{(+)} \hat{\Lambda} d^{4M} \vec{\lambda} \quad (10)$$

where

$$\mathcal{L}_A^{(+)} = -\frac{1}{2} \left[\hat{H}'_A(\boldsymbol{\alpha}, \boldsymbol{\beta} + \partial\boldsymbol{\alpha}) + \hat{H}'_N(\boldsymbol{\alpha} + \partial\boldsymbol{\beta}, \boldsymbol{\beta}) \right] \quad (11)$$

According to Eqs. (8) and (9), we also have

$$\mathcal{L}_A^{(+)} = -\frac{1}{2} \left[\hat{H}'_N(\boldsymbol{\beta} + \partial\boldsymbol{\alpha}, \boldsymbol{\alpha}) + \hat{H}'_N(\boldsymbol{\alpha} + \partial\boldsymbol{\beta}, \boldsymbol{\beta}) \right] \quad (12)$$

So

$$\begin{aligned} \mathcal{L}_A^{(+)} &= J \sum_{\langle i,j \rangle} \alpha_i \beta_j - \frac{U}{2} \sum_{i=1}^M \alpha_i^2 \beta_i^2 + \mu_e \sum_{i=1}^M \alpha_i \beta_i \\ &+ \frac{J}{2} \sum_{\langle i,j \rangle} (\alpha_i \partial_{\alpha_j} + \beta_i \partial_{\beta_j}) - \frac{U}{2} \sum_{i=1}^M n_i (\alpha_i \partial_{\alpha_i} + \beta_i \partial_{\beta_i}) \\ &+ \frac{\mu_e}{2} \sum_{i=1}^M (\alpha_i \partial_{\alpha_i} + \beta_i \partial_{\beta_i}) - \frac{U}{4} \sum_{i=1}^M (\alpha_i^2 \partial_{\alpha_i}^2 + \beta_i^2 \partial_{\beta_i}^2) \end{aligned} \quad (13)$$

Comparing Eq. (13) with Eq. (A7), we obtain

$$V = J \sum_{i,j} \omega_{ij} \alpha_i \beta_j - \frac{U}{2} \sum_{i=1}^M n_i^2 + \mu_e \sum_{i=1}^M n_i \quad (14)$$

$$A_j^{(+)} = \frac{J}{2} \sum_{i=1}^{2M} \omega_{ji} \alpha^i - \frac{U}{2} n_j \alpha^j + \frac{\mu_e}{2} \alpha^j, \quad j = 1, 2, \dots, 2M \quad (15)$$

$$D_{ij} = -\frac{U}{2} \delta_{ij} \alpha^{j2}, \quad i, j = 1, 2, \dots, 2M \quad (16)$$

where $\omega_{ij} = \delta_{i,j-1} + \delta_{i-1,j}$, $\omega_{i+M,j+M} = \omega_{ji}$ and $\omega_{i+M,j} = \omega_{i,j+M} = 0$. Also, the effective complex boson number is $n_i = n'_i + in''_i = \alpha_i \beta_i = n_{i+M}$. Considering Eq. (B8), we have

$$B_{ij} = i\sqrt{\frac{U}{2}} \delta_{ij} \alpha^j \quad (17)$$

Choosing the gauge $g_k = i\sqrt{\frac{U}{2}}(n'_k - |n_k|)$ [35] and considering Eq. (17), we can now calculate the Itô equations and convert them into the Stratonovich form of the Langevin equations (see appendix C for more calculations details). The Stratonovich stochastic equations, which are a natural physical choice [47] and more suitable for numerical solutions, compared to the Itô stochastic equations, and also have superior convergence properties [35, 48], are

$$\begin{aligned} d\Omega^{(S)} &= \Omega \left(V - \sum_{j=1}^M (g_j^2 - i\frac{U}{2}n''_j) \right) d\tau \\ &+ \Omega \sum_{k=1}^{2M} g_k dW_k \end{aligned} \quad (18)$$

$$\begin{aligned} d\alpha^{j(S)} &= \frac{J}{2} \sum_{i=1}^{2M} \omega_{ji} \alpha^i d\tau - \frac{U}{2} (|n_j| + in''_j) \alpha^j d\tau \\ &+ \frac{2\mu_e + U}{4} \alpha^j d\tau + i\sqrt{\frac{U}{2}} \alpha^j dW_j \end{aligned} \quad (19)$$

where the Wiener increments dW_i have the property [34, 49]

$$\langle dW_i(\tau) dW_j(s) \rangle_s = \delta_{ij} \delta(\tau - s) d\tau^2 \quad (20)$$

where $\langle \rangle_s$ means stochastic average.

II. SIMULATIONS AND COMPARISONS IN DIFFERENT LIMITING CASES

We simulate the 1D Bose-Hubbard model Stratonovich equations Eq. (19) using eXtensible Multi-Dimensional Simulator (XMDS) [64]. We use XMDS with the semi-implicit interaction picture SIIP method. We assume that at $\tau = 0$, there are N particles on average, in a thermal state [33] in the system. So the initial conditions are

$$\alpha_j = \sqrt{N/2}(\xi_l + i\xi_m), \quad \beta_j = \alpha_j^*, \quad \Omega = 1 \quad (21)$$

where ξ_l and ξ_m are random numbers with zero mean and standard deviation 1 which can be realised by Gaussian random numbers with zero mean and standard deviation 1 [33].

A. One-site model

Figure 1 compares the highly accurate numerical calculations, using a truncated number state basis, with the gauge P representation simulations for $M = 1$ [38]. It shows the independence of the expectation value of the number of particles $\langle \hat{n}_1 \rangle$ at the target temperature

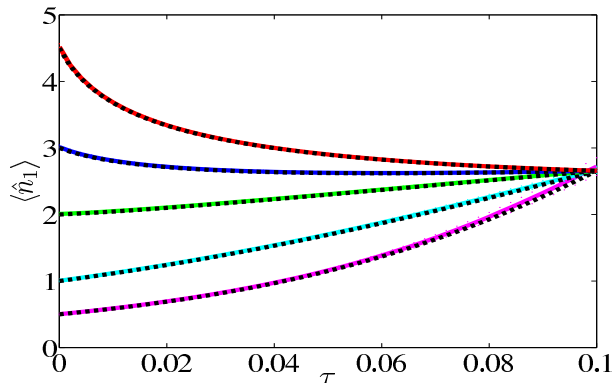


FIG. 1: Solid lines show the gauge P numerical calculations of $\langle \hat{n}_1 \rangle$ versus τ for $M = 1$, $J = 0$ and $n_0 = 0.5, 1, 2, 3$ and 4.5 . The target chemical potential μ_T is 0.5 . Solid, upper dotted, and lower dotted lines show simulation results $\langle \hat{n}_1 \rangle$, $\langle \hat{n}_1 \rangle + \sigma$ (sampling error) and $\langle \hat{n}_1 \rangle - \sigma$, respectively. Black dashed lines show the highly accurate numerical calculations using a truncated number-state basis.

$T = 10 U$ (here, $\tau_T = 0.1$) from the initial average number of particles n_0 , which is in good agreement with the numerical calculations based on a truncated number-state basis. As the figure shows, for a sufficiently large target imaginary time τ_T (sufficiently small temperature T) and a common value of the chemical potential μ_T , $\langle \hat{n}_1 \rangle$ is independent of the initial number of particles n_0 [37]. According to the figure, the expectation value of the number of particles at $\tau_T = 0.1$ is 2.66 , which is independent of the different initial values of $n_0 = 0.5, 1, 2, 3$ and 4.5 . Independence from the n_0 is very useful for the phase space simulations, because for different sets of the chemical potential and other parameters such as J and U the sampling error and also the stability of the simulations depends on n_0 .

Figure 2 shows the average number of particles, $\langle \hat{n}_1 \rangle$, versus the inverse temperature τ for the large value of $\tau_T = 20$. There is good agreement between the highly accurate numerical values and the gauge P simulation results. Figure 3 shows the simulation results for $\langle \hat{n}_1 \rangle$ as a function of the chemical potential μ_T . By decreasing the temperature sampling error is increased, specially at high values of the chemical potential. It is possible to reduce the sampling error by increasing the number of simulation trajectories. According to Fig. 3, the stepwise pattern of the average number of particles as a function of the chemical potential vanishes as the temperature is increased from $T = 0.1 U$ to $T = 10 U$. Because there is no hopping matrix element J , this result is valid for an array of M lattice sites in 1D, 2D and 3D. Therefore, for $J = 0$, in a system with M lattice sites in 1D, 2D and 3D, the stepwise pattern in the $\langle \hat{n}_i \rangle - \mu_T$ plot vanishes as the temperature is increased from $T = 0.1 U$ to $T = 10 U$. For the Bose-Hubbard model, according to Eqs. (8) and

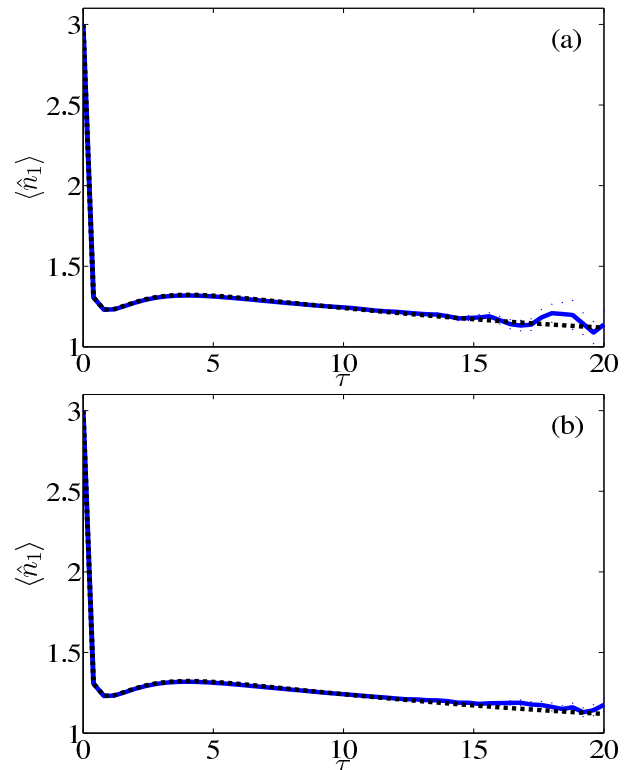


FIG. 2: $\langle \hat{n}_1 \rangle$ versus τ for $M = 1$, $n_0 = 3$, $J = 0$, $U = 1.0$, $d\tau = 10^{-3}$, $\mu_T = 0.9$ ($\mu_e = 0.9144$) and (a) $n_p = 2 \times 10^9$ and (b) $n_p = 2 \times 10^{10}$. Conventions as in Fig. 1.

(12), we have

$$\begin{aligned}
 -2\mathcal{L}_A^{(+)} &= -J \sum_{\langle i,j \rangle}^M \alpha_i (\beta_j + \partial_{\alpha_j}) \\
 &+ \frac{1}{2} U \sum_{i=1}^M \alpha_i^2 (\beta_i + \partial_{\alpha_i})^2 - \mu_e \sum_{i=1}^M \alpha_i (\beta_i + \partial_{\alpha_i}) \\
 &- J \sum_{\langle i,j \rangle}^M \beta_i (\alpha_j + \partial_{\beta_j}) + \frac{1}{2} U \sum_{i=1}^M \beta_i^2 (\alpha_i + \partial_{\beta_i})^2 \\
 &- \mu_e \sum_{i=1}^M \beta_i (\alpha_i + \partial_{\beta_i})
 \end{aligned} \tag{22}$$

B. Two-site model for $U = 0$

For $M = 2$, we have a double well and the Stratonovich equations can be written from Eq. (C13) and Eq. (19). Figure 4 shows $\langle \hat{n}_2 \rangle$ for a double site model ($M = 2$) with $U = 0$, $J = 1$, $n_0 = 5$ and $\mu_T/J = -1.01$ ($\mu_e/J = -0.9918$), where $\mu_T = -1.01$ is the target chemical potential at $T = 0.1 J$. This figure also compares the exact analytical results [38] with the gauge P simu-

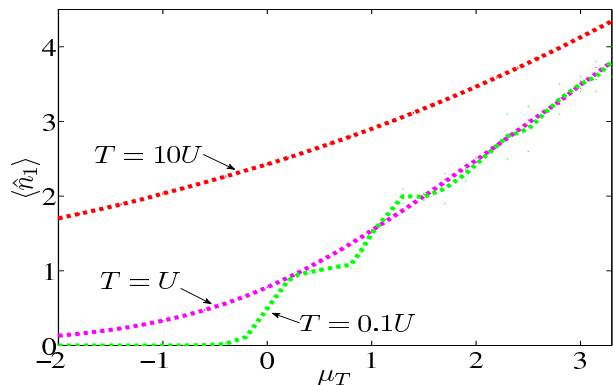


FIG. 3: Gauge P simulation of $\langle \hat{n}_1 \rangle$ versus μ_T , for $M = 1$, $n_0 = 1.2$, $J = 0$, $U = 1$ and three different values of τ_T . Here again, μ_T is the chemical potential at the target temperature T . As the temperatures is increased from $T = 0.1 U$ to $T = 10 U$, the stepwise pattern of the average number of particles versus the chemical potential, which is clearly seen below $T_0 = 0.06 U$ as a truncated number-state basis shows, vanishes. Dots around the diagram for $\tau_T = 10$ show the sampling error. For $T = U$ and $T = 10U$ sampling error is too small to be seen.

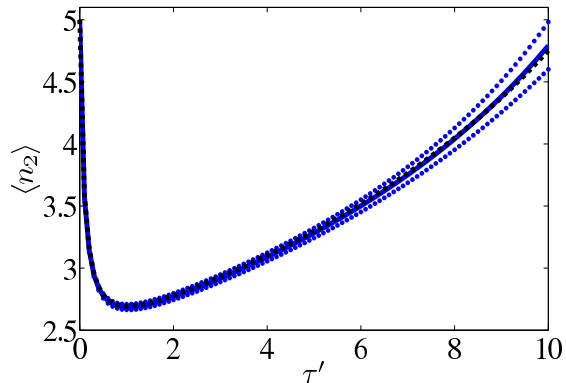


FIG. 4: Comparison of the simulation results for $\langle \hat{n}_2 \rangle$ with the analytical results, for $n_0 = 5$, $M = 2$, $U = 0$, $J = 1$ and $\mu_T/J = -1.01$ ($\mu_e/J = -0.9918$). Here, we have $\tau' = J/k_B T = 1/T$ and the number of the stochastic trajectories n_p is 10^5 . Other conventions as in Fig. 1.

lations and shows good agreement between them. The sampling error is due to the stochastic initial conditions given by Eq. (21).

C. Two-site model for $U \neq 0$ and $J \neq 0$

The simulation codes have been tested for the limiting cases when either $U = 0$ or $J \neq 0$ and are now ready for the general case of a two-site system in which both hopping matrix element J and the on-site interaction U exist. In Fig. 5 $\langle \hat{n}_2 \rangle$ (blue solid line), the rel-

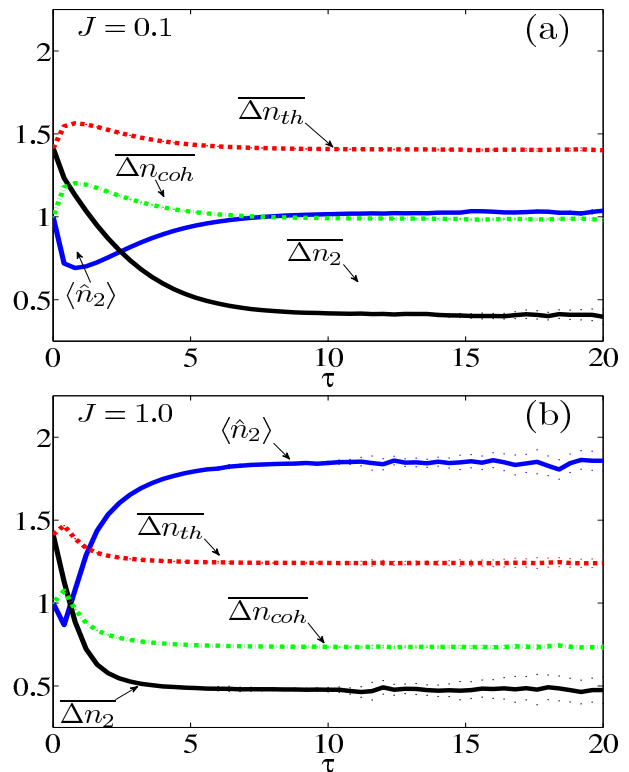


FIG. 5: Simulation results for the expectation values of the number of particles $\langle \hat{n}_2 \rangle$, the relative standard deviation $\overline{\Delta n_2} = \Delta n_2 / \langle \hat{n}_2 \rangle$, the relative standard deviation for a coherent state with the same number of particles $\overline{\Delta n_{coh}} = \Delta n_{coh} / \langle \hat{n}_2 \rangle$ and the relative standard deviation for a thermal state with the same number of particles $\overline{\Delta n_{th}} = \Delta n_{th} / \langle \hat{n}_2 \rangle$ at one of the sites in a double well system. τ is proportional to the inverse temperature and the dotted lines around each line show the sampling errors. Here, the stochastic averages have been taken over $n_p = 10^9$ trajectories and the target chemical potential μ_T is 0.5.

ative standard deviation $\overline{\Delta n_2} = \Delta n_2 / \langle \hat{n}_2 \rangle$ (black solid line), the relative standard deviation for a coherent state with the same number of particles $\overline{\Delta n_{coh}} = \Delta n_{coh} / \langle \hat{n}_2 \rangle$ (green dashed-dotted line) and the relative standard deviation for a thermal state with the same number of particles $\overline{\Delta n_{th}} = \Delta n_{th} / \langle \hat{n}_2 \rangle$ (red dashed line) in a double well system are shown, where $\Delta n_2 = \sqrt{\langle \hat{n}_2^2 \rangle - \langle \hat{n}_2 \rangle^2}$, $\Delta n_{coh} = \sqrt{\langle \hat{n}_2 \rangle}$ and $\Delta n_{th} = \sqrt{\langle \hat{n}_2 \rangle^2 + \langle \hat{n}_2 \rangle}$. Here the on-site interaction U is 1 and J/U in Fig. 5(a) and (b) is 0.1 and 1.0, respectively. In this quantum simulation, the number of trajectories, n_p , is 10^9 . Also, the target chemical potential, μ_T , is 0.5.

As Fig. 5(a) shows, when J/U is 0.1, the average number of particles at the temperature $T = 0.05 U$ ($\tau_T = 20$) is almost 1 which is close to the exact value of the average number of particles for $J/U = 0$, shown in Fig. ???. Note that, as we increase J/U to 1.0, at $\tau_T = 20$, we have $\langle \hat{n}_2 \rangle \simeq 1.8$. Also, if we increase the hopping matrix ele-

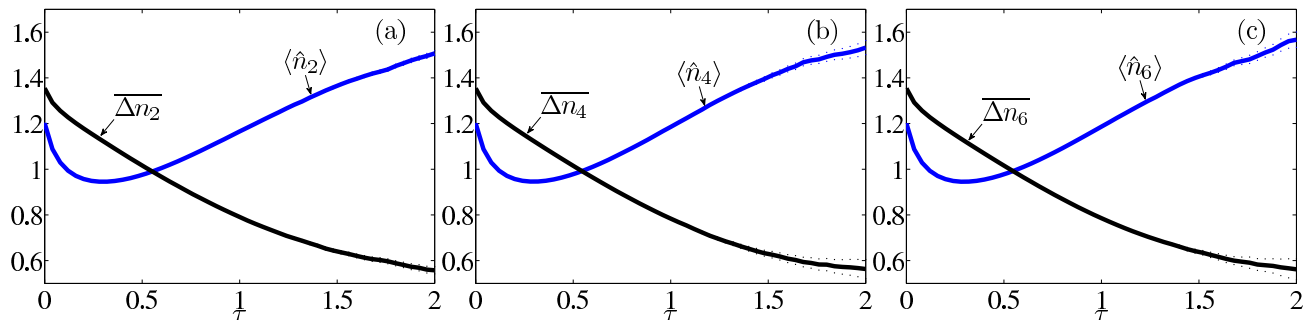


FIG. 6: $\langle \hat{n} \rangle$ and the relative standard deviation $\overline{\Delta n} = \Delta n / \langle \hat{n} \rangle$ for the hopping matrix element $J = 0.4$ and three different system sizes $M = 3, 7$ and 11 . Here, we also have $n_0 = 1.2$, $U = 1.0$ and $\mu_T = 0.5$. When the size of the system changes from 7 to 11, for the central sites, 4 and 6, respectively, the expectation values of the number of particles and especially the standard deviations, within the sampling error, are in good agreement.

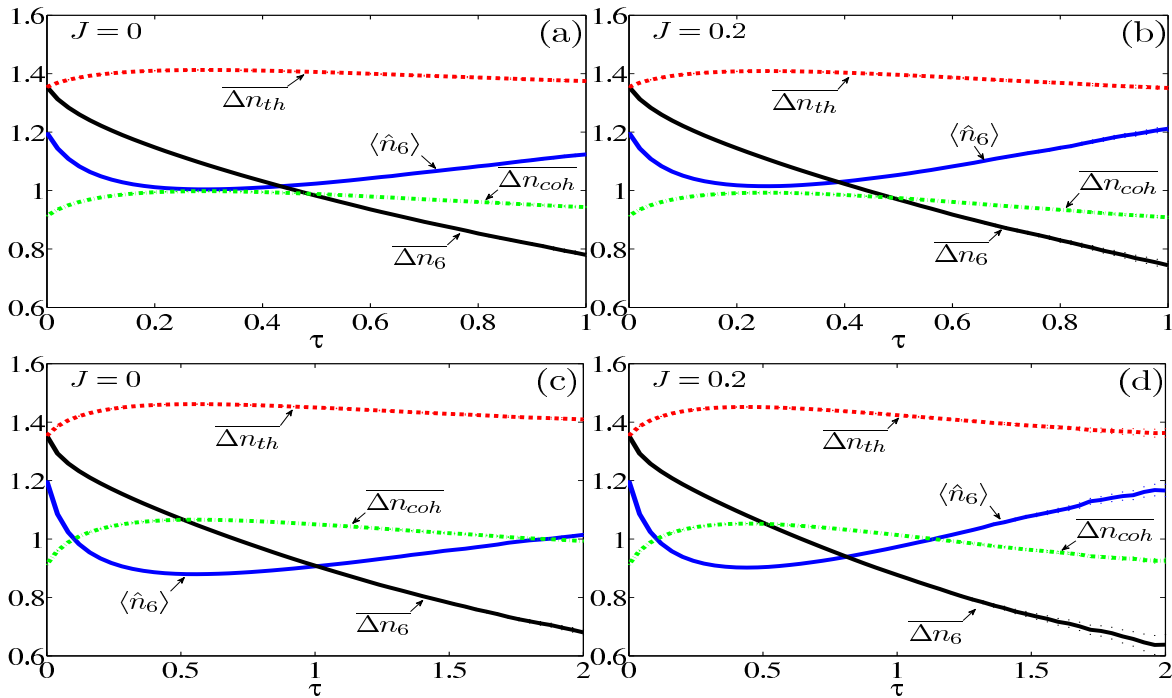


FIG. 7: $\langle \hat{n}_6 \rangle$ and the relative standard deviations, for a general state $\overline{\Delta n}_6$, a thermal state $\overline{\Delta n}_{th}$ and the coherent state $\overline{\Delta n}_{coh}$. Here we have $M = 11$, $n_0 = 1.2$, $U = 1.0$, $\mu_T = 0.5$ and (a) $J = 0$, $\tau_T = 1$, $n_p = 10^6$, (b) $J = 0.2$, $\tau_T = 1$, $n_p = 10^6$, (c) $J = 0$, $\tau_T = 2$, $n_p = 10^7$ and (d) $J = 0.2$, $\tau_T = 2$, $n_p = 10^7$.

ment the relative standard deviation $\overline{\Delta n}_2$ increases and in both cases for $J/U = 0.1$ and $J/U = 1.0$ we have

$$\overline{\Delta n}_2 < \overline{\Delta n}_{coh} < \overline{\Delta n}_{th} \quad (23)$$

It is interesting also that the relative standard deviation $\overline{\Delta n}_2$ approaches that of a coherent state as we move to large values of J/U which at low temperatures are in the superfluid regime. This is in the right direction for describing a superfluid as a coherent state.

III. SIMULATION OF M-SITE MODEL FOR $U \neq 0$ AND $J \neq 0$

For $M \geq 3$, the Stratonovich equations can be written from Eq. (C13) and Eq. (19). Figure 6 compares $\langle \hat{n} \rangle$ and $\overline{\Delta n} = \Delta n / \langle \hat{n} \rangle$ at the central site for three different system sizes with the hopping matrix element $J = 0.4$. This figure shows that the size effect is not very considerable for $M = 11$ as, within the sampling error, the values of $\langle \hat{n} \rangle$ and $\overline{\Delta n}$ are similar to those for $M = 7$ and, in particular the relative number fluctuations are the same. Therefore, a Bose-Hubbard model with $M = 11$ may be

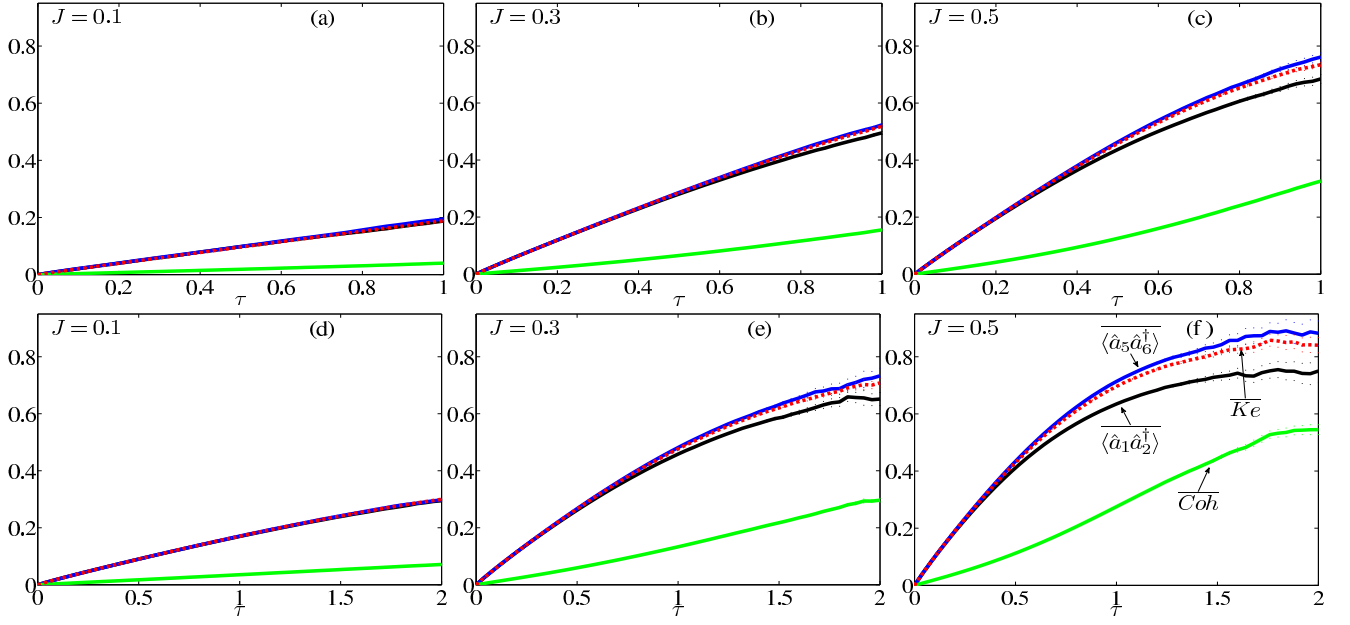


FIG. 8: This figure shows relative values of the coherence between sites, $\overline{Coh} = Coh / \langle \hat{n}_6 \rangle$, $\overline{Ke} = Ke / \langle \hat{n}_6 \rangle$, $\overline{\langle \hat{a}_1 \hat{a}_2^\dagger \rangle} = \langle \hat{a}_1 \hat{a}_2^\dagger \rangle / \langle \hat{n}_6 \rangle$ and $\overline{\langle \hat{a}_5 \hat{a}_6^\dagger \rangle} = \langle \hat{a}_5 \hat{a}_6^\dagger \rangle / \langle \hat{n}_6 \rangle$ at two different target temperatures $T = U$ in (a) and (c) and $T = 0.5 U$ in (b) and (d). The labels in (a)-(c) are the same as in (d). By decreasing the target temperature (increasing τ_T) \overline{Coh} , \overline{Ke} , $\overline{\langle \hat{a}_1 \hat{a}_2^\dagger \rangle}$ and $\overline{\langle \hat{a}_5 \hat{a}_6^\dagger \rangle}$ increase. Also, at a constant temperature, by increasing the hopping matrix element, all of these measures of the coherence between lattice sites increase.

large enough to approximately represent the behaviour of an infinite system. In Fig. 7 the relative standard deviations $\overline{\Delta n_6}$, , are plotted versus the inverse temperature, τ , for a general state and are compared with those of an ideal thermal state $\overline{\Delta n_{th}}$, where $(\Delta n_{th} = \sqrt{\langle \hat{n} \rangle^2 + \langle \hat{n} \rangle})$, and a coherent state $\overline{\Delta n_{coh}}$, where $(\Delta n_{coh} = \sqrt{\langle \hat{n} \rangle})$ for two different values of J/U . In order to obtain Δn for the thermal and the coherent states we have used the simulation results for $\langle \hat{n} \rangle$. According to the plots, at a constant low temperature, as J/U is increased, the standard deviation increases. Also the standard deviation at the target temperature T and the target chemical potential μ_T for both different values of J/U is less than the standard deviation for a coherent state and much less than that of a thermal state. Also because at low values of J/U the atoms form a superfluid, when the temperature goes to zero, the closeness of the standard deviation $\overline{\Delta n_6}$ to $\overline{\Delta n_{coh}}$ supports the idea of describing a superfluid by a coherent state. Also an increase in the (quantum) standard deviation $\langle n \rangle$ is observed as the temperature increases.

Because the number of atoms changes with temperature, it is important to know the behaviour of the measures of the coherence relative to the average number of atoms per lattice site. Figure 8 shows relative coherences

$\overline{\langle \hat{a}_1 \hat{a}_2^\dagger \rangle} = \langle \hat{a}_1 \hat{a}_2^\dagger \rangle / \langle \hat{n}_6 \rangle$ and $\overline{\langle \hat{a}_5 \hat{a}_6^\dagger \rangle} = \langle \hat{a}_5 \hat{a}_6^\dagger \rangle / \langle \hat{n}_6 \rangle$ and also $\overline{Coh} = Coh / \langle \hat{n}_6 \rangle$ and $\overline{Ke} = Ke / \langle \hat{n}_6 \rangle$, where Coh and Ke are defined as

$$Coh = \left\langle \frac{1}{M(M-1)} \sum_{i,j} \hat{a}_i^\dagger \hat{a}_j \right\rangle \quad (24)$$

$$Ke = \left\langle \frac{1}{2(M-1)} \sum_i (\hat{a}_i^\dagger \hat{a}_{i+1} + \hat{a}_i \hat{a}_{i+1}^\dagger) \right\rangle \quad (25)$$

Coh and Ke show coherence between all lattice sites and between all the adjacent sites, respectively. According to Eqs. (1) and (24), between the expectation value of the kinetic energy part of the Bose-Hubbard Hamiltonian

$$KE = -J \sum_i^{M-1} \left\langle (\hat{a}_i^\dagger \hat{a}_{i+1} + \hat{a}_i \hat{a}_{i+1}^\dagger) \right\rangle \quad (26)$$

and Ke , Eq. (25), which is an average of the coherence between adjacent sites, there is a simple relation

$$Ke = \frac{-KE}{2J(M-1)}, \quad M \neq 1 \quad (27)$$

As Fig. 8 shows, the relative coherence between sites 1 and 2, $\overline{\langle \hat{a}_1 \hat{a}_2^\dagger \rangle}$, is different from that between sites 5

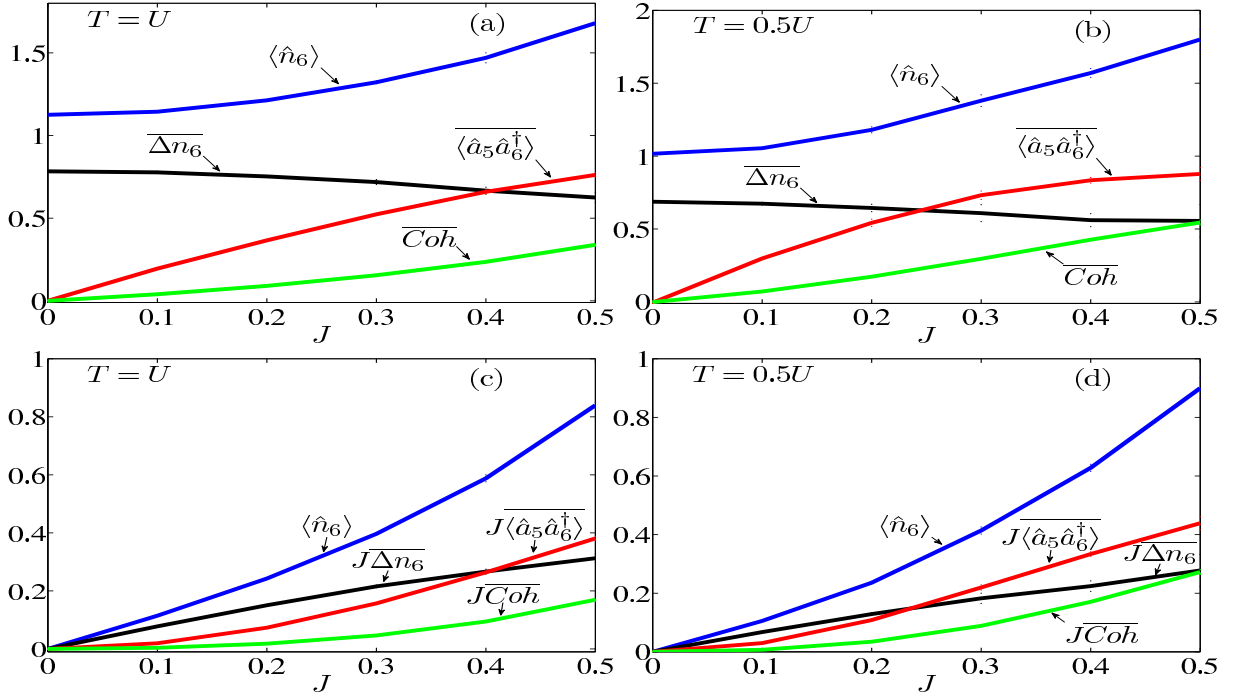


FIG. 9: $\langle \hat{n}_6 \rangle$ and the relative values $\overline{\Delta n_6}$, $\overline{\langle \hat{a}_5 \hat{a}_6^\dagger \rangle}$, \overline{Coh} , $J\langle \hat{n}_6 \rangle$, $J\overline{\Delta n_6}$, $J\overline{\langle \hat{a}_5 \hat{a}_6^\dagger \rangle}$ and $J\overline{Coh}$ as a function of J for two different target temperatures $T = 0.5U$ and $T = U$. All lines are to guide the eye. The sampling error, which is small, is shown by the dots along the lines.

and 6, $\overline{\langle \hat{a}_5 \hat{a}_6^\dagger \rangle}$, due to the edge (size) effect. Because the edge effect in a system with size $M = 11$ is small and all the other adjacent sites, except sites 1 and 2, have almost the same coherence (or same relative coherence) between each other as exists between sites 5 and 6, we have, according to Fig. 8, at temperatures $T_1 = U$ and $T_2 = 0.5 U$ (within the sampling error)

$$Ke = \langle \hat{a}_5 \hat{a}_6^\dagger \rangle \quad (28)$$

According to Eq. (25) and Fig. 8, for a Bose-Hubbard model with $M=11$ sites in 1D, at temperatures $T_1 = U$ and $T_2 = 0.5 U$, the kinetic energy of the system is simply $KE = -20J \langle \hat{a}_5 \hat{a}_6^\dagger \rangle$.

In general, for M lattice sites, the kinetic energy term KE , Eq. (26), is given by $-2J(M-1) \langle \hat{a}_{M/2} \hat{a}_{(M+2)/2}^\dagger \rangle$ for even M and $-2J(M-1) \langle \hat{a}_{(M-1)/2} \hat{a}_{(M+1)/2}^\dagger \rangle$ for odd $M \geq 3$.

In Fig. 8, all the parameters show an increase when either the system is cooled or the hopping matrix element J is increased. By decreasing the temperature at a constant J the relative coherence increases; therefore the ultracold bosons approach a superfluid state where the coherence between the lattice sites is very high. When the constant temperature is low enough, decreasing the tunnelling rate takes the system to a Mott insulator phase

where coherence between the sites is lost [2, 3]. Figure 9 shows $\langle \hat{n}_6 \rangle$ and the relative values $\overline{\Delta n_6}$, $\overline{\langle \hat{a}_5 \hat{a}_6^\dagger \rangle}$, \overline{Coh} , $J\langle \hat{n}_6 \rangle$, $J\overline{\Delta n_6}$, $J\overline{\langle \hat{a}_5 \hat{a}_6^\dagger \rangle}$ and $J\overline{Coh}$ as a function of J for two different temperatures. Here again, according to the figure, all the parameters increase when either the temperature is reduced or the hopping matrix element J is increased.

Figure 10 shows $\overline{C_2(r)} = C_2(r) / \langle \hat{n}_6 \rangle$ as a function of τ . All values of $\overline{C_2(r)}$ show an increase when T is reduced. The same behaviour is observed when J is increased.

According to Figs. 8 and 10, all relative measures of the coherence \overline{Coh} , \overline{Ke} , $\overline{\langle \hat{a}_1 \hat{a}_2^\dagger \rangle}$, $\overline{\langle \hat{a}_5 \hat{a}_6^\dagger \rangle}$ and $\overline{C_2(r)}$ increase when either the temperature is reduced or the hopping matrix element is increased.

IV. CALCULATION OF THE LUTTINGER PARAMETER

The important parameter which has been used to locate the critical parameters of the superfluid to Mott insulator quantum phase transition is atom-atom correlations $C(r) = \langle \hat{a}_0^\dagger \hat{a}_r \rangle$ [22, 23] and more generally $C_i(r) = \langle \hat{a}_i^\dagger \hat{a}_{i+r} \rangle$ against J [45].

According to Refs. [39, 40, 41], basically, it is possi-

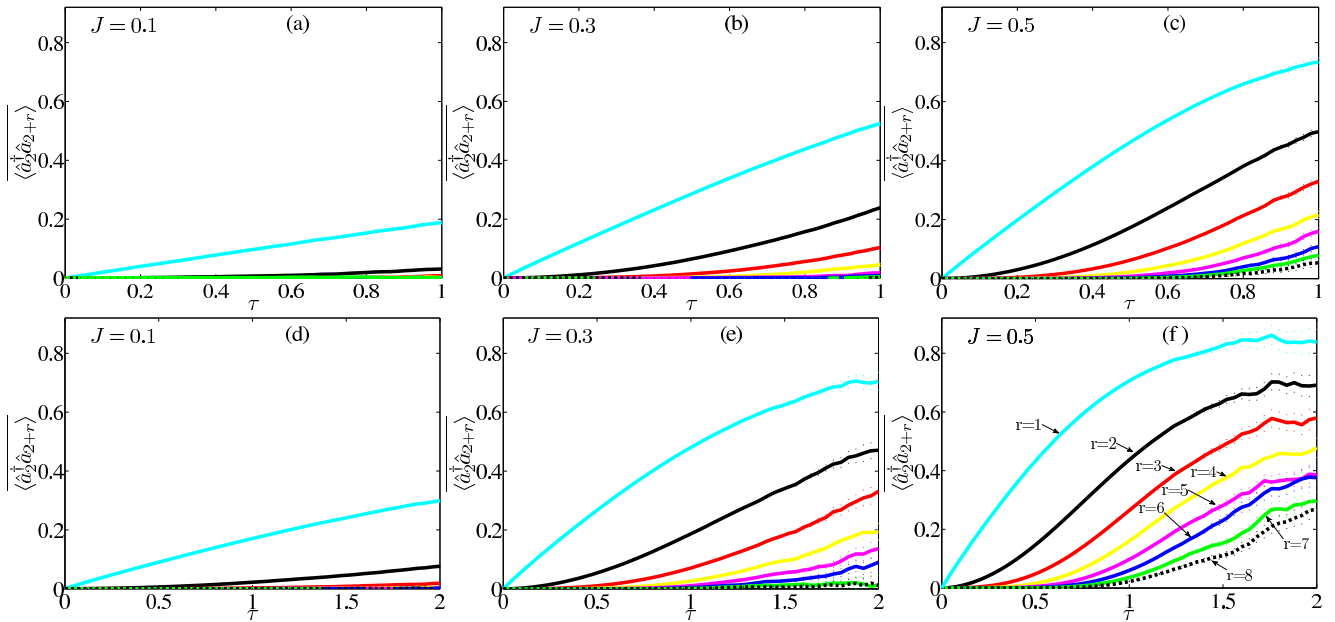


FIG. 10: Relative atom-atom correlations $\overline{C_2(r)} = C_2(r) / \langle \hat{n}_6 \rangle$ as a function of τ for $M=11$, $\mu_\tau = 0.5$, values of $J = 0.3$ and 0.5 and two different target temperatures $T = U$ in (a) and (c) and $T = 0.5U$ in (b) and (d). The labels in (a)-(c) are the same as in (d). The relative atom-atom correlations increase when either the temperature is reduced or the hopping matrix element is increased.

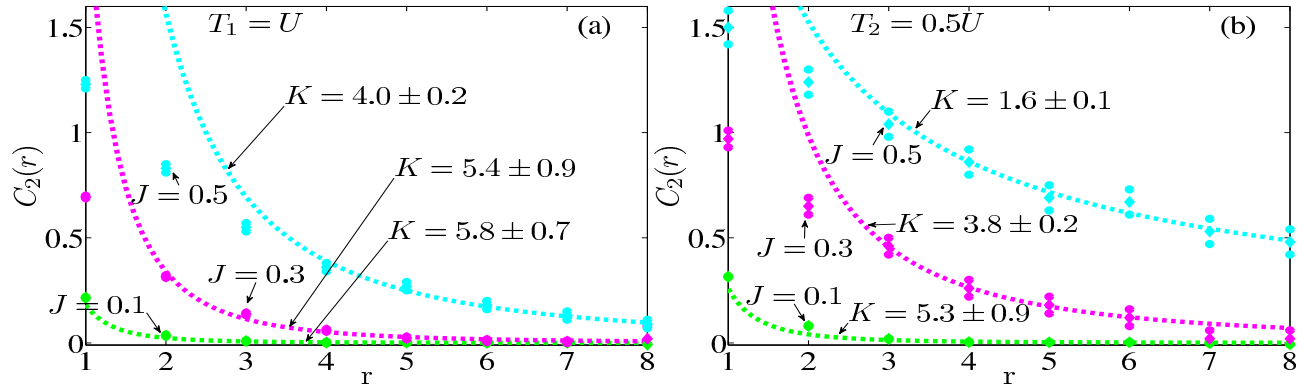


FIG. 11: Atom-atom correlations $C_2(r)$ as a function of r , where r is the site number, for $M=11$, $\mu_\tau = 0.5$ and two different target temperatures (a) $T = U$ and (b) $T = 0.5U$ and values of $J = 0.1, 0.3$ and 0.5 . Diamonds and circles around them show the simulation results and their sampling error, respectively. Dashed lines, which look like dotted lines, are fits to the function $r^{-K/2}$ where K is the Luttinger parameter. According to this figure, $C_2(r)$ increases as temperature is decreased. Also at a constant temperature by increasing the hopping matrix element J , coherence between sites increases. Moreover, as J is increased the Luttinger parameter K decreases.

ble to fit the function $r^{-K/2}$ to the curve of $C_2(r)$ as a function of r for different values of the chemical potential and hopping matrix element, find the boundaries of the Mott lobes, and obtain the phase diagram of the Bose-Hubbard model. Figure 11 shows the atom-atom correlations $C_2(r)$ as a function of r for $T = U$ and $T = 0.5U$. At each temperature three different values of the hopping matrix element J are considered. According to this figure, $C_2(r)$ increases as the temperature is decreased. Also at a constant temperature by increasing the hopping

matrix element J , the coherence between sites increases. Moreover, as J is increased the Luttinger parameter K decreases. At $\mu_\tau/U = 0.5$ and at the constant temperatures $T_1 = U$ and $T_2 = 0.5U$, by increasing the hopping matrix element J , relative atom-atom correlations $\overline{C_2(r)}$, where $C_2(r) = \langle \hat{a}_2^\dagger \hat{a}_{2+r} \rangle$, which are other measures of the relative coherence between sites, increase but the Luttinger parameter K , which is important in locating the boundaries of the Mott-insulator lobes, decreases.

Also, for a constant value of the hopping matrix element $J = 0.5$, by reducing the temperature from $T_1 = U$ to $T_2 = 0.5 U$, the Luttinger parameter K changes from 4.0 ± 0.2 to 1.6 ± 0.1 .

V. CONCLUSION

In this paper, using the Bose-Hubbard model, we simulated ultracold atoms in the grand canonical ensemble of quantum degenerate gases. We studied ultracold atoms at finite temperatures with the gauge P representation. We have written a simulation code using XMDS, which generates a C++ code. In 1D we simulated the Bose-Hubbard model with 1, 2, 3, 7 and 11 sites.

The simulation results are in good agreement with highly accurate numerical calculations, based on a truncated number-state basis, when there is no on-site interaction between atoms. Also, for a double well system, we compared the simulation results with exact analytical results for the case where the atoms can tunnel between sites but the on-site interaction between the sites is zero.

We also investigated the average number of particles, relative standard deviations and coherences between sites at finite temperatures for the Bose-Hubbard model in 1D with open boundary conditions consisting of 1, 2, 3, 7 and 11 sites and showed that at non-zero temperatures the relative standard deviation is not zero even for $J/U = 0$ and grows as J/U is increased. We found that the relative standard deviation $\overline{\Delta n_i}$ is higher at higher temperatures and is less than the corresponding relative standard deviation for a coherent state and is much less than that of a thermal state with the same value of $\langle \hat{n}_i \rangle$.

For $J = 0$, we showed that above $T = 0.1 U$ the step-wise pattern in the plot of $\langle \hat{n}_i \rangle$ versus the target chemical potential μ_T starts to vanish; therefore, there is no Mott insulator-like lobe in the phase diagram of the Bose-Hubbard model in the plane of μ/U - J/U .

Comparing the Bose-Hubbard model with $M = 3, 7$ and 11, we showed that in a 1D Bose-Hubbard model with $M = 11$ and open boundary conditions edge effects are insignificant except for the side sites (the first and last sites).

At low temperatures, for constant values of $J/U = 0.2$ and $\mu_T/U = 0.5$, by reducing the temperature from $T_1 = U$ to $T_2 = 0.5 U$, the relative standard deviation of the number of particles at each lattice $\overline{\Delta n_i}$ decreases but remains well below those of a coherent state, $\overline{\Delta n_{coh}}$, and also a thermal state, $\overline{\Delta n_{th}}$, with the same average number of particles. The relative standard deviation $\overline{\Delta n_i}$ is closer to $\overline{\Delta n_{coh}}$ than to $\overline{\Delta n_{th}}$. This confirms that the ground state of a superfluid can be described by a coherent state.

For $\mu_T/U = 0.5$, at the constant temperatures $T_1 = U$ and $T_2 = 0.5 U$, the relative standard deviation $\overline{\Delta n_i}$ decreases as J/U is reduced. At these temperatures the lowest value of the relative standard deviation of the number of particles at each lattice $\overline{\Delta n_i}$ is not zero even

if the tunnelling is zero. This confirms that at these temperatures, for $J/U = 0$, the compressibility κ is not zero, so there is no Mott insulator phase present at these temperatures. This is in good agreement with the temperature $T = 0.1 U$ discussed above or, more accurately, with the melting temperature $T_0 = 0.06 U$ above which there is no Mott insulator phase in the Bose-Hubbard model [38].

At the constant temperatures $T_1 = U$ and $T_2 = 0.5 U$, for $\mu_T/U = 0.5$, by increasing the tunnelling rate all physical quantities \overline{Coh} , \overline{Ke} , $\langle \hat{a}_1 \hat{a}_2^\dagger \rangle$, $\langle \hat{a}_5 \hat{a}_6^\dagger \rangle$ and $\overline{C_2(r)}$, which measure *relative coherence* between the lattice sites, increase. Also, if J/U is kept constant but the temperature is reduced from $T_1 = U$ to $T_2 = 0.5 U$, all of them increase. Likewise, all measures of *coherence* increase when either the temperature is reduced or the hopping matrix element is increased.

For a Bose-Hubbard model with $M=11$ sites in 1D, at temperatures $T_1 = U$ and $T_2 = 0.5 U$, the kinetic energy part of the system is simply given by $-20J \langle \hat{a}_5 \hat{a}_6^\dagger \rangle$, within the sampling error, which can be generalised to $KE = -2J(M-1) \langle \hat{a}_{M/2} \hat{a}_{(M+2)/2}^\dagger \rangle$, for an even number of lattice sites M , and to $KE = -2J(M-1) \langle \hat{a}_{(M-1)/2} \hat{a}_{(M+1)/2}^\dagger \rangle$ for an odd number of lattice sites M .

At $\mu_T/U = 0.5$ and at the constant temperatures $T_1 = U$ and $T_2 = 0.5 U$, by increasing the hopping matrix element J , the Luttinger parameter K , which is important in locating the boundaries of the Mott-insulator lobes, decreases. Also, by reducing the temperature from $T_1 = U$ to $T_2 = 0.5 U$, for a constant value of the hopping matrix element $J = 0.5$ the Luttinger parameter K changes from 4.0 ± 0.2 to 1.6 ± 0.1 .

With the particular gauge-choice used here, we have found that the the growth of sampling error is a limiting factor at low temperatures and a large number of sites. However, it is always possible that for particular situations a better choice of gauge may reduce the sampling error.

Even with the sampling error limitations described above, the gauge-P method is very general and could potentially be applied to a range of ultracold lattice systems, including

1. The J/U critical ratios and phase diagrams in 1D, 2D, and 3D, for the Bose-Hubbard model and also the critical values and phase diagrams of the superfluid to Mott insulator quantum phase transition at zero temperature.
2. Disordered Bose-Hubbard model [2, 50, 51, 52] and also two component bosons in periodic lattices [51, 53].
3. The coexistence of the Mott insulator and superfluid phases in inhomogeneous traps, such as quadratic and quartic trapping potentials, for a

continuous range of incommensurate fillings [54, 55].

4. Ultracold bosons in a double-well potential [56] and a tilted multi-level double-well potential [57].
5. Extended Bose-Hubbard models [58].
6. Strongly interacting bosons in a 2D rotating square lattice which can also be studied via a modified Bose-Hubbard Hamiltonian [59].

Appendix A: Positive P representation

There are density operators for which the P representation does not exist. For example, the P representation cannot describe nonclassical effects such as squeezing or antibunching [33]. In contrast, the positive P representation gives stochastic differential equations which can represent genuine quantum-mechanical problems like squeezing or antibunching [60, 61, 62].

In the positive P representation, we can write [34]

$$\hat{\rho} = \int P(\boldsymbol{\alpha}, \boldsymbol{\beta}, \tau) \hat{\Lambda} d^{4M} \vec{\lambda} \quad (\text{A1})$$

where $\vec{\lambda} = (\boldsymbol{\alpha}, \boldsymbol{\beta}) = (\alpha_1, \alpha_2, \dots, \alpha_M, \beta_1, \beta_2, \dots, \beta_M)$ and

$$\hat{\Lambda} = \frac{|\boldsymbol{\alpha}\rangle\langle\boldsymbol{\beta}^*|}{\langle\boldsymbol{\beta}^*|\boldsymbol{\alpha}\rangle} = \|\boldsymbol{\alpha}\rangle\langle\boldsymbol{\beta}^*||e^{-\boldsymbol{\alpha}\cdot\boldsymbol{\beta}} \quad (\text{A2})$$

$|\boldsymbol{\alpha}\rangle$ is an M -dimensional Bargmann coherent state [33] and $|\alpha_i\rangle = e^{|\alpha_i|/2} |\alpha_i\rangle$, where M is the number of modes (number of lattice sites, for example), τ may represent real time or imaginary time (inverse temperature) and

$$|\alpha_i\rangle = \exp\left(-\frac{1}{2}|\alpha_i|^2\right) \sum_{n=0}^{\infty} \frac{\alpha_i^n}{n!} |n\rangle, \quad (\text{A3})$$

where $i = 1, 2, \dots, M$. We also have the identities

$$\begin{aligned} \hat{\mathbf{a}}\hat{\Lambda} &= \boldsymbol{\alpha}\hat{\Lambda}, & \hat{\mathbf{a}}^\dagger\hat{\Lambda} &= \left[\boldsymbol{\beta} + \frac{\partial}{\partial\boldsymbol{\alpha}}\right]\hat{\Lambda}, \\ \hat{\Lambda}\hat{\mathbf{a}} &= \left[\boldsymbol{\alpha} + \frac{\partial}{\partial\boldsymbol{\beta}}\right]\hat{\Lambda}, & \hat{\Lambda}\hat{\mathbf{a}}^\dagger &= \boldsymbol{\beta}\hat{\Lambda}. \end{aligned} \quad (\text{A4})$$

Expectation values of the normally ordered products $\hat{a}_i^{\dagger m} \hat{a}_i^n$ can be written in the positive P representation as the following

$$\langle \hat{a}_i^{\dagger m} \hat{a}_i^n \rangle = \int \beta_i^m \alpha_i^n P(\boldsymbol{\alpha}, \boldsymbol{\beta}, \tau) \hat{\Lambda} d^{4M} \vec{\lambda} \quad (\text{A5})$$

Also, after integration by parts, provided the boundary terms vanish at infinity, we can write

$$\int \frac{\partial P(\boldsymbol{\alpha}, \boldsymbol{\beta}, \tau)}{\partial\tau} \hat{\Lambda} d^{4M} \vec{\lambda} = \int P(\boldsymbol{\alpha}, \boldsymbol{\beta}, \tau) \mathcal{L}_A^{(+)} \hat{\Lambda} d^{4M} \vec{\lambda} \quad (\text{A6})$$

When there are no terms higher than second order, $\mathcal{L}_A^{(+)}$ may be expanded as

$$\mathcal{L}_A^{(+)} = V + A_j^{(+)} \partial_j + \frac{1}{2} D_{ij} \partial_i \partial_j \quad (\text{A7})$$

In the positive P representation, the Fokker-Planck equation is given by

$$\frac{\partial P(\boldsymbol{\alpha}, \boldsymbol{\beta}, \tau)}{\partial\tau} = (V - \partial_j A_j^{(+)} + \frac{1}{2} \partial_i \partial_j D_{ij}) P(\boldsymbol{\alpha}, \boldsymbol{\beta}, \tau) \quad (\text{A8})$$

Appendix B: Gauge P representation

In the gauge P representation, the density matrix can be written as [35]

$$\hat{\rho} = \int G(\vec{\alpha}, \tau) \hat{\Lambda} d^{4M+2} \vec{\alpha} \quad (\text{B1})$$

where $\vec{\alpha} = (\alpha^0, \alpha^1, \dots, \alpha^M, \alpha^{M+1}, \alpha^{M+2}, \dots, \alpha^{2M}) = (\Omega, \boldsymbol{\alpha}, \boldsymbol{\beta})$, and

$$\hat{\Lambda} = \Omega \frac{|\boldsymbol{\alpha}\rangle\langle\boldsymbol{\beta}^*|}{\langle\boldsymbol{\beta}^*|\boldsymbol{\alpha}\rangle} = \Omega \|\boldsymbol{\alpha}\rangle\langle\boldsymbol{\beta}^*||e^{-\boldsymbol{\alpha}\cdot\boldsymbol{\beta}} \quad (\text{B2})$$

When $\Omega = 1$, this phase space representation reduces to the positive P representation [35]. Here, we have the identities given by Eq. (A4) plus $\Omega \frac{\partial}{\partial\Omega} \hat{\Lambda} = \hat{\Lambda}$.

In this phase space representation, quantum averages of the normally ordered products $\hat{a}_i^{\dagger m} \hat{a}_i^n$ are

$$\langle \hat{a}_i^{\dagger m} \hat{a}_i^n \rangle = \frac{\langle \beta_i^m \alpha_i^n \Omega + (\alpha_i^m \beta_i^n \Omega)^* \rangle_{stoch}}{\langle \Omega + \Omega^* \rangle_{stoch}} \quad (\text{B3})$$

where $\langle f(\boldsymbol{\alpha}) \rangle_{stoch} = \int f(\boldsymbol{\alpha}) G(\vec{\alpha}, \tau) d^{4M+2} \vec{\alpha}$.

After integration by parts, provided the boundary terms vanish at infinity, we have

$$\int \frac{\partial G(\vec{\alpha}, \tau)}{\partial\tau} \hat{\Lambda} d^{4M+2} \vec{\alpha} = \int G(\vec{\alpha}, \tau) \mathcal{L}_{GA} \hat{\Lambda} d^{4M+2} \vec{\alpha} \quad (\text{B4})$$

In the gauge P representation, when there are no terms higher than second order, \mathcal{L}_{GA} may be expanded as

$$\mathcal{L}_{GA} = \mathcal{L}_A^{(+)} + \left[V + \frac{1}{2} \vec{g} \cdot \vec{g} \Omega \partial_\Omega + g_k B_{jk} \partial_j \right] (\Omega \partial_\Omega - 1) \quad (\text{B5})$$

$$\mathcal{L}_{GA} = A_\mu \partial_\mu + \frac{1}{2} \underline{D}_{\mu\nu} \partial_\mu \partial_\nu, \quad \mu, \nu = 0, 1, 2, \dots, 2M \quad (\text{B6})$$

where $\mathcal{L}_A^{(+)}$ is given by Eq. (A7), $\vec{g} = \{g_i(\vec{\alpha})\}$ are $2M$ arbitrary gauge functions and

$$\vec{A} = (A_0, A_1, \dots, A_{2M}), \quad A_0 = \Omega V, \quad A_j = A_j^{(+)} - g_k B_{jk} \quad (\text{B7})$$

$$\mathbf{D} = \mathbf{B}\mathbf{B}^T, \quad \underline{\mathbf{D}} = \underline{\mathbf{B}}\underline{\mathbf{B}}^T, \quad \underline{\mathbf{B}} = \begin{pmatrix} 0 & \Omega \vec{g} \\ 0 & \mathbf{B} \end{pmatrix} \quad (\text{B8})$$

Now, the Itô form [47] of the Langevin equations are

$$d\Omega = \Omega \left(V d\tau + \sum_{k=1}^{2M} g_k dW_k \right), \quad (\text{B9})$$

$$d\alpha^j = \left(A_j^{(+)} - \sum_{k=1}^{2M} g_k B_{jk} \right) d\tau + \sum_{k=1}^{2M} B_{jk} dW_k, \quad (\text{B10})$$

where $j = 1, 2, \dots, 2M$ and the Wiener increments dW_i have the property $\langle dW_i(\tau) dW_j(s) \rangle_s = \delta_{ij} \delta(\tau - s) d\tau^2$ [34, 49] which can be realized at each $d\tau$ by real Gaussian noises with zero average and variance $d\tau$.

Appendix C: Itô and Stratonovich forms of the Langevin equations

Considering Eqs. (B9) and (B10) for the Bose-Hubbard model, Itô Langevin equations are

$$d\Omega = \Omega \left(J \sum_{i,j} \omega_{ij} \alpha_i \beta_j - \frac{U}{2} \sum_{i=1}^M n_i^2 + \mu_e \sum_{i=1}^M n_i \right) d\tau + \Omega \sum_{k=1}^{2M} g_k dW_k \quad (\text{C1})$$

$$d\alpha^j = \left[\frac{J}{2} \sum_{i=1}^{2M} \omega_{ji} \alpha^i - \frac{U}{2} (|n_j| + in_j'') \alpha^j + \frac{\mu_e}{2} \alpha^j \right] d\tau + i \sqrt{\frac{U}{2}} \alpha^j dW_j, \quad j = 1, 2, \dots, 2M. \quad (\text{C2})$$

The Stratonovich stochastic equations are [47]

$$d\alpha^{\mu(S)} = \left(A_\mu^{(S)} \right) d\tau + \sum_{k=1}^{2M} B_{\mu k} dW_k, \quad (\text{C3})$$

where $A_\mu^{(S)} = A_\mu - \frac{S_\mu}{2}$, $\mu = 0, 1, 2, \dots, 2M$ and

$$S_\mu = \sum_{\nu=0}^{2M} \sum_{\gamma=0}^{2M} \left(\underline{\underline{B}}_{\gamma\nu} \partial_{\alpha^\gamma} + \underline{\underline{B}}_{\gamma\nu}^* \partial_{\alpha^{\gamma*}} \right) \underline{\underline{B}}_{\mu\nu} \quad (\text{C4})$$

Because $\underline{\underline{B}}_{\mu 0}$ is zero, we can write

$$S_\mu = S_\mu^1 + S_\mu^2 \quad (\text{C5})$$

where

$$S_\mu^1 = \sum_{j=1}^{2M} \left(\underline{\underline{B}}_{0j} \partial_\Omega + \underline{\underline{B}}_{0j}^* \partial_{\Omega^*} \right) \underline{\underline{B}}_{\mu j} \quad (\text{C6})$$

$$S_\mu^2 = \sum_{j=1}^{2M} \sum_{k=1}^{2M} \left(\underline{\underline{B}}_{kj} \partial_{\alpha^k} + \underline{\underline{B}}_{kj}^* \partial_{\alpha^{k*}} \right) \underline{\underline{B}}_{\mu j} \quad (\text{C7})$$

We have $\underline{\underline{B}}_{0j} = \Omega g_j$, $\partial_\Omega \underline{\underline{B}}_{0j} = g_j$, $\partial_{\Omega^*} \underline{\underline{B}}_{0j} = 0$, $\underline{\underline{B}}_{ij} = i \sqrt{\frac{U}{2}} \delta_{ij} \alpha^j$, so

$$S_0^1 = \Omega \sum_{j=1}^{2M} g_j^2 \quad (\text{C8})$$

Also

$$\begin{aligned} S_0^2 &= \sum_{j=1}^{2M} \sum_{k=1}^{2M} \left(\underline{\underline{B}}_{kj} \partial_{\alpha^k} + \underline{\underline{B}}_{kj}^* \partial_{\alpha^{k*}} \right) \underline{\underline{B}}_{0j} \\ &= i\Omega \sqrt{\frac{U}{2}} \sum_{j=1}^{2M} \sum_{k=1}^{2M} \left(\delta_{kj} \alpha^j \partial_{\alpha^k} - \delta_{kj} \alpha^{j*} \partial_{\alpha^{k*}} \right) g_j \\ &= i\Omega \sqrt{\frac{U}{2}} \sum_{k=1}^{2M} \left(\alpha^k \partial_{\alpha^k} - \alpha^{k*} \partial_{\alpha^{k*}} \right) g_k \\ &= i\Omega \sqrt{\frac{U}{2}} \sum_{k=1}^M [(\alpha_k \partial_{\alpha_k} + \beta_k \partial_{\beta_k}) - (\alpha_k^* \partial_{\alpha_k^*} + \beta_k^* \partial_{\beta_k^*})] g_k \\ &= i\Omega \sqrt{\frac{U}{2}} \sum_{k=1}^M [(\alpha_k \partial_{\alpha_k} + \beta_k \partial_{\beta_k}) - (\alpha_k^* \partial_{\alpha_k^*} + \beta_k^* \partial_{\beta_k^*})] \\ &\quad \times i \sqrt{\frac{U}{2}} (n_k' - |n_k|) = -i\Omega U \sum_{k=1}^M n_k'' \quad (\text{C9}) \end{aligned}$$

Considering Eq. (C8), we obtain

$$S_0 = \Omega \sum_{j=1}^M (2g_j^2 - iU n_j'') \quad (\text{C10})$$

Furthermore, $\partial_\Omega \underline{\underline{B}}_{ij} = \partial_{\Omega^*} \underline{\underline{B}}_{ij} = 0$ which, according to Eq. (C5), gives $S_i^1 = 0$. Moreover

$$\begin{aligned} S_i^2 &= -\frac{U}{2} \sum_{j=1}^{2M} \sum_{k=1}^{2M} (\delta_{kj} \alpha^j \partial_{\alpha^k} \delta_{ij} - \delta_{kj} \alpha^{j*} \partial_{\alpha^{k*}} \delta_{ij}) \alpha^j \\ &= -\frac{U}{2} \alpha^i \quad (\text{C11}) \end{aligned}$$

Therefore, we have $S_i = -\frac{U}{2} \alpha^i$. The Stratonovich equations, Eq. (C3), are now

$$\begin{aligned} d\Omega^{(S)} &= \Omega \left(V d\tau + \sum_{k=1}^{2M} g_k dW_k \right) - \frac{S_0}{2} d\tau \\ &= \Omega \left[\left(V - \sum_{j=1}^M (g_j^2 - i \frac{U}{2} n_j'') \right) d\tau + \sum_{k=1}^{2M} g_k dW_k \right] \quad (\text{C12}) \end{aligned}$$

$$\begin{aligned} d\alpha^{j(S)} &= \left[\frac{J}{2} \sum_{i=1}^{2M} \omega_{ji} \alpha^i - \frac{U}{2} (|n_j| + in_j'') \alpha^j + \frac{\mu_e}{2} \alpha^j \right] d\tau \\ &\quad - \frac{S_j}{2} d\tau + i \sqrt{\frac{U}{2}} \alpha^j dW_j \\ &= \left[\frac{J}{2} \sum_{i=1}^{2M} \omega_{ji} \alpha^i - \frac{U}{2} (|n_j| + in_j'') \alpha^j + \frac{2\mu_e + U}{4} \alpha^j \right] d\tau \\ &\quad + i \sqrt{\frac{U}{2}} \alpha^j dW_j \quad (\text{C13}) \end{aligned}$$

Acknowledgments

We would like to thank Peter Drummond, Peter Zoller, Matthias Troyer, Alexander Mering, Daniel Heinzen, Pe-

ter Hannaford, Bryan Dalton and Chris Vale for helpful discussions. This project is supported by the ARC Centre of Excellence for Quantum Atom Optics and a Swinburne University Strategic Initiative fund.

-
- [1] P. D. Drummond, P. Deuar, and K. V. Kheruntsyan, Phys. Rev. Lett. **92**, 040405 (2004).
- [2] M. P. A. Fisher, P. B. Weichman, G. Grinstein, and D. S. Fisher, Phys. Rev. B **40**, 546 (1989).
- [3] D. Jaksch, C. Bruder, J. I. C. C. W, Gardiner, and P. Zoller, Phys. Rev. Lett. **81**, 3108 (1998).
- [4] M. Greiner, O. Mandel, T. Esslinger, T. W. Hänsch, and I. Bloch, Nature **415**, 39 (2002).
- [5] S. Ghanbari, T. D. Kieu, A. Sidorov, and P. Hannaford, J. Phys. B: At. Mol. Opt. Phys. **39**, 847 (2006).
- [6] S. Ghanbari, T. D. Kieu, and P. Hannaford, J. Phys. B: At. Mol. Opt. Phys. **40**, 1283 (2007).
- [7] R. Gerritsma, S. Whitlock, T. Fernholz, H. Schlatter, J. A. Luigjes, J.-U. Thiele, J. B. Goedkoop, and R. J. C. Spreeuw, Phys. Rev. A **76**, 033408 (pages 6) (2007).
- [8] M. Singh, M. Volk, A. Akulshin, A. Sidorov, R. McLean, and P. Hannaford, J. Phys. B: At. Mol. Opt. Phys. **41**, 065301 (2008).
- [9] S. Whitlock, R. Gerritsma, T. Fernholz, and R. J. C. Spreeuw, New Journal of Physics **11**, 023021 (2009).
- [10] S. Ghanbari, P. B. Blakie, P. Hannaford, and T. D. Kieu, Eur. Phys. J. B **70**, 3305 (2009).
- [11] C. Bruder, R. Fazio, and G. Schön, Ann. Phys. **14**, 566 (2005).
- [12] G. G. Batrouni, R. T. Scalettar, and G. T. Zimanyi, Phys. Rev. Lett. **65**, 1765 (1990).
- [13] G. G. Batrouni and R. T. Scalettar, Phys. Rev. B **46**, 9051 (1992).
- [14] V. A. Kashurnikov, A. V. Krasavin, and B. V. Svistunov, Pisma Zh. Eksp. Teor. Fiz. **64**, 92 (JETP Lett. **64**, 99), 1996).
- [15] M. Capello, F. Becca, M. Fabrizio, and S. Sorella, Phys. Rev. Lett. **99**, 056402 (pages 4) (2007).
- [16] K. Sheshadri, H. R. Krishnamurthy, R. Pandit, and T. V. Ramakrishnan, Europhys. Lett. **22**, 257 (1993).
- [17] D. van Oosten, P. V. D. Straten, and H. T. C. Stoof, Phys. Rev. A **63**, 053601 (2001).
- [18] M. O. Oktel, M. Nita, and B. Tanatar, Phys. Rev. B **75**, 045133 (pages 7) (2007).
- [19] W. Krauth, Phys. Rev. B **44**, 9772 (1991).
- [20] V. F. Elesin, V. A. Kashurnikov, and L. A. Openov, JETP Lett. **60**, 177 (1994).
- [21] J. K. Freericks and H. Monien, Phys. Rev. B **53**, 2691 (1996).
- [22] T. D. Kühner and H. Monien, Phys. Rev. B **58**, R14741 (1998).
- [23] T. D. Kühner, S. R. White, and H. Monien, Phys. Rev. B **61**, 12474 (2000).
- [24] V. A. Kashurnikov and B. V. Svistunov, Phys. Rev. B **53**, 11776 (1996).
- [25] S. R. White, Phys. Rev. Lett. **69**, 2863 (1992).
- [26] P. Corboz, A. Kleine, F. F. Assaad, I. P. McCulloch, U. Schollwck, and M. Troyer, arXiv:0707.4394v1 [cond-mat.str-el] (2007).
- [27] P. Buonsante and A. Vezzani, Phys. Rev. A **70**, 033608 (pages 8) (2004).
- [28] X. L. X and Y. Yu, Phys. Rev. A **74**, 063615 (pages 6) (2006).
- [29] M. C. Cha and J. W. Lee, Phys. Rev. Lett. **98**, 266406 (pages 4) (2007).
- [30] B. Schmidt, L. I. Plimak, and M. Fleischhauer, Phys. Rev. A **71**, 041601 (2005).
- [31] L. I. Plimak, M. K. Olsen, and M. Fleischhauer, Phys. Rev. A **70**, 013611 (2004).
- [32] X. Lu, J. Li, and Y. Yu, Physical Review A (Atomic, Molecular, and Optical Physics) **73**, 043607 (pages 12) (2006), URL <http://link.aps.org/abstract/PRA/v73/e043607>.
- [33] C. W. Gardiner and P. Zoller, *Quantum Noise, 3rd Ed.* (Springer, Heidelberg, Berlin, Germany, 2004).
- [34] P. D. Drummond and C. W. Gardiner, J. Phys. A: Math. Gen. **13**, 2353 (1980).
- [35] P. Deuar and P. D. Drummond, Phys. Rev. A **66**, 033812 (2002).
- [36] P. Deuar and P. D. Drummond, J. Phys. A: Math. Gen. **39**, 2723 (2006).
- [37] P. Deuar, PhD thesis, The University of Queensland, Available at <http://www.physics.uq.edu.au/people/deuar/thesis/> (2004).
- [38] S. Ghanbari, PhD thesis, Swinburne University of Technology, Melbourne, Australia (2008).
- [39] T. Giamarchi and A. J. M. A. J, Phys. Rev. B **46**, 9325 (1992).
- [40] T. Giamarchi, Physica B **975**, 230 (1997).
- [41] L. I. Glazman and A. I. Larkin, Phys. Rev. Lett. **79**, 3736 (1997).
- [42] O. Morsch and M. Oberthaler, Rev. Mod. Phys. **78**, 179 (pages 37) (2006).
- [43] G. H. Wannier, Phys. Rev. **52**, 191 (1937).
- [44] S. Liu, H. Xiong, B. Lu, and M. Zhan, J. Phys. B: At. Mol. Opt. Phys. **40**, 517 (2007).
- [45] B. Damski and J. Zakrzewski, Phys. Rev. A **74**, 043609 (pages 6) (2006).
- [46] L. I. P. M. K. Olsen and M. Fleischhauer, Phys. Rev. A **70**, 013611 (pages 7) (2004).
- [47] C. W. Gardiner, *Handbook of Stochastic Methods, 2nd Ed.* (Springer, Berlin, Germany, 1985).
- [48] P. D. Drummond and I. K. Mortimer, J. Comput. Phys. **93**, 144 (1991), ISSN 0021-9991.
- [49] P. Deuar and P. D. Drummond, J. Phys. A: Math. Gen. **39**, 1163 (2006).
- [50] K. V. Krutitsky, A. Pelster, and R. Graham, New J. Phys. **8**, 187 (2006).
- [51] R. Roth and K. Burnett, J. Opt. B: Quantum Semiclass. Opt. **5**, S50 (2003).
- [52] P. Buonsante, V. Penna, A. Vezzani, and P. B. Blakie, Phys. Rev. A **76**, 011602 (pages 4) (2007).
- [53] E. Altman, W. Hofstetter, E. Demler, and M. D. Lukin, New J. Phys. **5**, 113 (2003).

- [54] G. G. Batrouni, V. Rousseau, R. T. Scalettar, M. Rigol, A. Muramatsu, P. J. H. Denteneer, and M. Troyer, *Phys. Rev. Lett.* **89**, 117203 (2002).
- [55] O. Gygi, H. G. Katzgraber, M. Troyer, S. Wessel, and G. G. Batrouni, *Phys. Rev. A* **73**, 063606 (pages 7) (2006).
- [56] G. J. Milburn, J. Corney, E. M. Wright, and D. F. Walls, *Phys. Rev. A* **55**, 4318 (1997).
- [57] D. R. Dounas-Frazer, A. M. Hermundstad, and L. D. Carr, *Phys. Rev. Lett.* **99**, 200402 (pages 4) (2007).
- [58] R. V. Pai and R. Pandit, *Phys. Rev. B* **71**, 104508 (pages 8) (2005).
- [59] R. Bhat, M. J. Holland, and L. D. Carr, *Phys. Rev. Lett.* **96**, 060405 (pages 4) (2006).
- [60] S. J. Carter, M. D. Reid, R. M. Shelby, and P. D. Drummond, *Phys. Rev. Lett.* **58**, 1841 (1987).
- [61] P. D. Drummond, R. M. Shelby, S. R. Friberg, and Y. Yamamoto, *Nature* **365**, 307 (1993).
- [62] P. D. Drummond and Z. Ficek, *Quantum Squeezing* (Springer, Berlin, Germany, 2004).
- [63] Instead of the long expression ‘the standard deviation of the number of particles’, for brevity, we may use the short term ‘standard deviation’.
- [64] Available at <http://www.physics.uq.edu.au/xmds/index.html>